

Granular aluminum: A superconducting material for high impedance quantum circuits

Lukas Grünhaupt,^{1,*} Martin Spiecker,^{1,*} Daria Gusenkova,¹ Nataliya Maleeva,¹
Sebastian T. Skacel,^{1,2} Ivan Takmakov,^{1,2,3} Francesco Valenti,^{1,4} Patrick
Winkel,¹ Hannes Rotzinger,¹ Alexey V. Ustinov,^{1,3} and Ioan M. Pop^{1,2,†}

¹*Physikalisches Institut, Karlsruhe Institute of Technology, 76131 Karlsruhe, Germany*

²*Institute of Nanotechnology, Karlsruhe Institute of Technology, 76344 Eggenstein-Leopoldshafen, Germany*

³*Russian Quantum Center, National University of Science and Technology MISIS, 119049 Moscow, Russia*

⁴*Institute for Data Processing and Electronics, Karlsruhe Institute of Technology, 76344 Eggenstein-Leopoldshafen, Germany*

(Dated: September 28, 2018)

Superconducting quantum information processing machines are predominantly based on microwave circuits with relatively low characteristic impedance, of about 100 Ohm, and small anharmonicity, which can limit their coherence and logic gate fidelity. A promising alternative are circuits based on so-called superinductors, with characteristic impedances exceeding the resistance quantum $R_Q = 6.4 \text{ k}\Omega$. However, previous implementations of superinductors, consisting of mesoscopic Josephson junction arrays, can introduce unintended nonlinearity or parasitic resonant modes in the qubit vicinity, degrading its coherence. Here we present a fluxonium qubit design using a granular aluminum (grAl) superinductor strip. Granular aluminum is a particularly attractive material, as it self-assembles into an effective junction array with a remarkably high kinetic inductance, and its fabrication can be in-situ integrated with standard aluminum circuit processing. The measured qubit coherence time T_2^R up to $30 \mu\text{s}$ illustrates the potential of grAl for applications ranging from protected qubit designs to quantum limited amplifiers and detectors.

Building large scale quantum information processing machines using superconducting circuits [1, 2] remains a challenging physics and engineering endeavor. Although there are promising small-scale prototypes [3–8] and proof of principle demonstrations for the necessary building blocks, such as error corrected qubits [9, 10] or remote entanglement protocols [11–14], scaling up to large numbers of logical qubits will require breakthroughs in all aspects of qubit technology, including qubit architecture and materials. As an example, one of the major challenges facing prevalent transmon qubit [15] processors is the problem of quantum state leakage towards non-computational degrees of freedom [16], which could become a roadblock for scaling. The limited anharmonicity of the transmon may be insufficient to isolate in frequency the qubit computational space from the surrounding, increasingly complex, microwave environment.

A promising alternative qubit architecture is based on so-called superinductors, with characteristic impedance larger than $R_Q = h/(2e)^2 = 6.4 \text{ k}\Omega$, such as the fluxonium qubit [17], which offers orders of magnitude larger anharmonicity, and coherence comparable to transmon qubits [18]. In these circuits, quantum fluctuations of the phase dominate over charge fluctuations, and provide a playground for the design of new, potentially protected quantum circuits [19–25]. Large inductors could also become a building block of next generation flux and phase qubits [26–28]. Moreover, microwave resonators employing superinductors and small capacitors have recently been used to boost and confine voltage fluctuations, enabling strong coupling between photons and the

electron orbitals in gate-defined quantum dots [29–31]. They could also be used in the near future to achieve strong coupling between photons and magnetic moments [32]. Last but not least, high characteristic impedance elements can be a resource for building tailored environments for transport measurements [33–36].

However, superinductors are not easy to obtain. One typically relies on the kinetic inductance of an array of tens to hundreds of Josephson junctions [17, 29, 37, 38], patterned in a compact geometry, to reduce stray capacitance. Although there are encouraging results [18, 39, 40], the experimental progress has been slowed down by the complexity in fabrication and microwave design required for junction based superinductors.

In this Letter we present a significantly simplified superinductor design based on an emerging material in the quantum circuits community: granular aluminum (grAl). To prove that a grAl superinductor operates as designed, and to quantify its quantum coherence, we use it to build a fluxonium qubit, which we operate and characterize using the tools of circuit quantum electrodynamics (cQED) [41]. The observed qubit spectrum is in agreement with the one expected from numerical diagonalization of the system Hamiltonian [42]. The measured quantum state coherence time T_2^R up to $30 \mu\text{s}$ recommends grAl as a competitive alternative to superinductors implemented with mesoscopic Josephson junction arrays, or thin films from other disordered superconductors, like NbN [43], NbTiN [30, 31, 44], or TiN [45, 46].

Granular aluminum is compatible and convenient to use with current Josephson junction fabrication technology [47, 48] used for pure aluminum circuits, because grAl simply self-assembles when depositing aluminum in a controlled oxygen atmosphere. Depending on the oxygen partial pressure, the deposition rate, and sub-

* Both authors contributed equally.

† ioan.pop@kit.edu

strate temperature, superconducting films with resistivities ranging from 10 to $10^4 \mu\Omega\text{cm}$ and critical temperatures of up to 3.15 K can be achieved [49, 50]. The kinetic inductance of grAl strips is proportional to their normal state resistance. It can therefore be tuned over a wide range, reaching values up to $\sim \text{nH}/\square$, while maintaining internal quality factors on the order of 10^5 in the single photon regime [51–53]. Moreover, the Kerr non-linearity can be reduced by orders of magnitude [54] compared to superinductors made of mesoscopic Josephson junction arrays [55], which helps to suppress the unwanted coupling between the qubit and the environment.

Figure 1a) shows the equivalent circuit of the fluxonium qubit coupled to the readout resonator. Shunting a Josephson junction (L_J, C_J) with a large, linear inductor (L_q), leads to an offset charge insensitive superconducting qubit, with a transition frequency tunable over several GHz, and comparable anharmonicity [17]. By inductively coupling (via L_s) the qubit to a readout resonator (L_r, C_r), we can measure the qubit state through the shift it induces on the resonator frequency [56]. In Fig. 1b) we show an optical microscope image of the readout resonator. We place the circuit in a copper rectangular waveguide sample holder, to which the resonator couples via its electric dipole moment, following the scheme reported in Ref. [57].

We fabricate the entire circuit comprised of readout resonator and fluxonium in a single electron-beam lithography, three-angle evaporation, lift-off process on a double-side polished c-plane sapphire substrate (see Supplemental Material for technical details). By employing the Niemeyer-Dolan technique [47, 48] and an asymmetric undercut [58] we pattern a conventional Al/AIOx/Al Josephson junction and its short connecting wires [cf. blue highlighted regions in Fig. 1e)]. Subsequently, without breaking vacuum, we perform the zero angle deposition of the 40 nm thick grAl film of the superinductor, with sheet resistance $R_s \approx 0.2 \text{ k}\Omega/\square$ at room temperature. The corresponding $0.8 \times 10^3 \mu\Omega\text{cm}$ resistivity is one order of magnitude below the values at which grAl undergoes a superconducting to insulating transition [49].

The hermetically sealed rectangular waveguide sample holder, anchored to the 25 mK stage of a commercial dilution cryostat, is placed inside a copper-aluminum shield covered with infrared absorbing coating and further enclosed by a μ -metal shield (cf. Ref. [53]). To measure the fluxonium spectrum we perform standard two-tone microwave spectroscopy, measuring the complex reflection coefficient S_{11} of the resonator, while sweeping a second generator in the range of expected qubit frequencies. Figure 2 shows the measured fluxonium spectrum (red points), Φ_0 periodic as a function of the external flux Φ_{ext} . From a numerical fit (cf. black line in Fig. 2) of the fluxonium Hamiltonian to the measured transition frequencies, we extract the total inductance of the loop $L_q + L_s = 225.6 \text{ nH}$, corresponding to a sheet inductance $L_{\text{kin}} = 0.1 \text{ nH}/\square$, the junction capacitance $C_J = 5.2 \text{ fF}$, and the Josephson inductance $L_J = 13.2 \text{ nH}$.

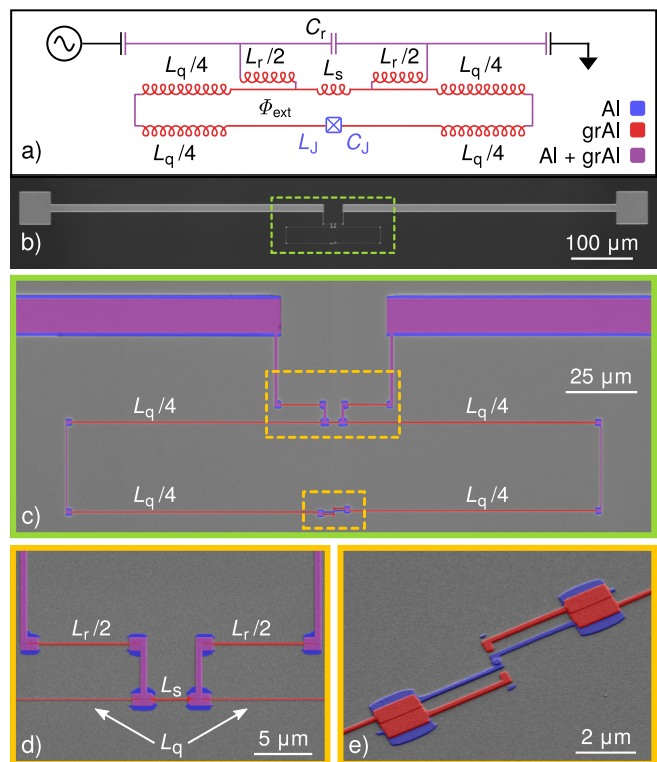


Figure 1. Fluxonium qubit built using a grAl superinductor. **a)** The qubit consists of a Josephson junction shunted by a $300 \mu\text{m}$ long grAl superinductor with an estimated characteristic impedance $Z \gtrsim 10 \text{ k}\Omega$ and the first self-resonant mode at 17.4 GHz (see Supplemental Material). To perform dispersive readout, we couple the qubit to a microwave resonator through a shared inductance $L_s \approx 1 \text{ nH}$. The color legend indicates the material used for each circuit element. **b)** Optical microscope image of the readout resonator, which couples to a rectangular waveguide sample holder (not shown) via its dipole moment, following Ref. [57]. **c)** False colored optical microscope image of the fluxonium qubit inductively coupled to the resonator [cf. green highlighted region in b)]. The circuit's inductors are all realized by grAl strips (highlighted in red). **d)** Scanning electron microscope (SEM) image of the resonator-qubit coupling [cf. top orange box in c)]. The resonator frequency, coupling strength, and qubit spectrum can all be independently tuned by the length of the corresponding grAl strips. **e)** Tilted SEM image of the fluxonium junction [cf. bottom orange box in c)]. Using a three angle electron beam lift-off process, we connect in-situ a conventional Al/AIOx/Al Josephson junction (highlighted in blue) to the grAl superinductor (see Supplemental Material). We estimate the junction area $A_J \approx 0.06 \mu\text{m}^2$.

The lower panel of Fig. 2 shows the shift of the readout resonator frequency vs. externally applied flux Φ_{ext} through the fluxonium loop, relative to the dressed resonator frequency of 7.278 GHz . We estimate a qubit state dependent dispersive shift of the resonator frequency in the range of 130 kHz at $\Phi_{\text{ext}}/\Phi_0 = -0.5$ (cf. color scale in Fig. 2 and the resonator linewidth of 3.2 MHz).

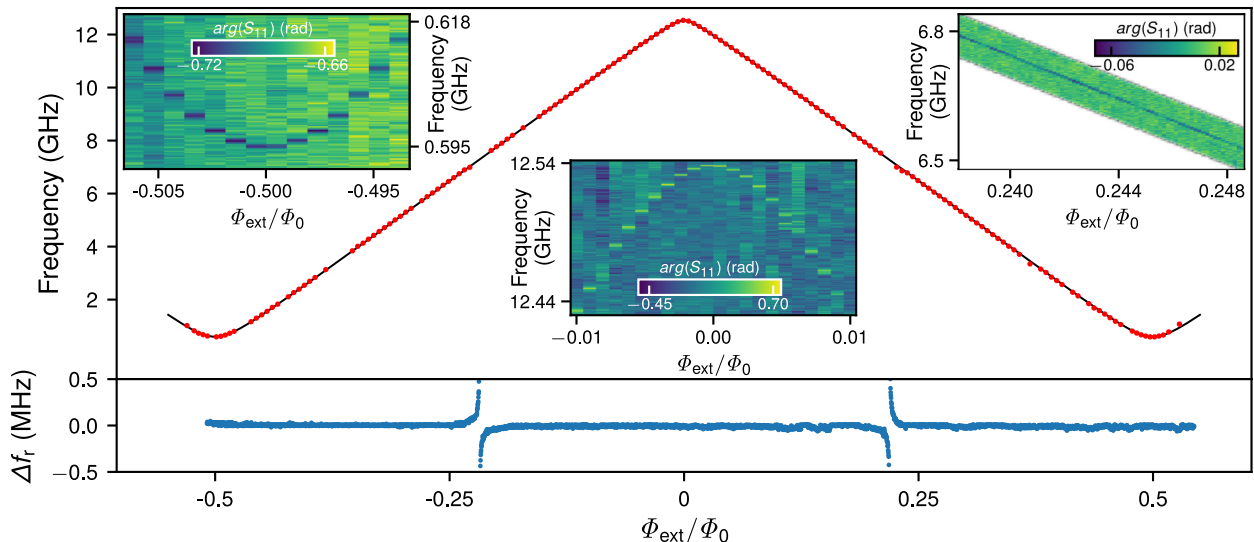


Figure 2. Fluxonium and readout resonator spectroscopy. Upper panel: Red points show the qubit transition frequency as a function of the external flux measured by two-tone spectroscopy. The solid black line is a fit of the fluxonium Hamiltonian following Ref. [42]. We extract a fluxonium inductance $L_q + L_s = 225.6$ nH, capacitance $C_J = 5.2$ fF, and Josephson inductance $L_J = 13.2$ nH. Changing the external magnetic flux Φ_{ext} through the fluxonium loop from half integer to integer flux quanta Φ_0 tunes the qubit transition frequency from $f_{0.5}^q = 0.594$ GHz to $f_0^q = 12.538$ GHz. The top-left and middle insets show zoom-ins into the extremal points of the spectrum at $\Phi_{\text{ext}}/\Phi_0 = -0.5$ and $\Phi_{\text{ext}} = 0$, respectively. As also visible from the narrowing spectral linewidth, the qubit transition frequency becomes first order flux noise independent at these two symmetry points. In the top-right inset we show qubit spectroscopy measurements ranging over 300 MHz for a flux bias close to $\Phi_{\text{ext}}/\Phi_0 = 0.25$. We do not observe anti-crossings, which would be signatures of a strong coupling to two-level defects, one of the mechanisms limiting superconducting qubit coherence [59]. Lower panel: Change of the readout resonator frequency at 7.278 GHz as a function of the external applied flux Φ_{ext} through the fluxonium loop. As the qubit frequency crosses the readout resonator frequency, we observe an anti-crossing of about 3 MHz.

To quantify the quantum coherence of the grAl fluxonium qubit we perform standard time-domain manipulations and measurements (see the Supplemental Material for a detailed setup schematic). Figure 3 shows the results obtained at the $\Phi_{\text{ext}}/\Phi_0 = -0.5$ sweet spot, where energy relaxation due to non-equilibrium quasiparticles tunneling through the Josephson junction is suppressed [18], the spectrum is first order flux noise insensitive [62] and the qubit coherence time shows a maximum [see Fig. 3c)]. We extract typical energy relaxation times T_1 in the range of 20 μs to 30 μs , and Ramsey coherence times T_2^{R} up to 30 μs .

By performing Rabi oscillations [60] with constant microwave drive power and varying duration, we achieve qubit population inversion with a frequency of 38 MHz, which corresponds to a π -pulse of ~ 13 ns [see lower left inset in Fig. 3a)], orders of magnitude faster than the coherence time.

We measured the relaxation time T_1 of the grAl fluxonium repeatedly, performing a total of 6000 measurements over the course of ~ 17 h. The averaged measurement result plotted in log-lin scale in Fig. 3a) shows an exponential behavior, and the histogram of the individual measurements is shown in the upper right inset

in Fig. 3a). From the distribution we obtain an average $T_1 = (23 \pm 4)$ μs . The measured T_1 values could be limited either by dielectric losses or by non-equilibrium quasiparticles [63–67] in the grAl superinductor [53, 68]. If excess quasiparticles in the grAl superinductor are the limiting loss mechanism at the $\Phi_{\text{ext}}/\Phi_0 = -0.5$ sweet spot, we extract a normalized density $x_{\text{qp}} = 4.1 \times 10^{-7}$ (following the methodology in Ref. [18]). This value is two orders of magnitude higher than previously observed in a Josephson junction array superinductor [18], but also one order of magnitude lower than values measured in grAl resonators [53]. The quasiparticle density in grAl is presumably increased compared to pure aluminum, due to the longer quasiparticle lifetime [53].

A spin-echo measurement performed by introducing a π -pulse in the middle of the Ramsey sequence increases T_2^{E} up to 46 μs , close to the theoretical limit of $T_2 = 2T_1$. We extract a dephasing time, dominated by low frequency noise, $T_\phi = 2T_1T_2^{\text{R}}/(2T_1 - T_2^{\text{R}}) \approx 72$ μs . The fluctuations of T_2^{R} can be due to residual magnetic flux noise, adsorbed surface spins [69], or the effect of fluctuating non-equilibrium quasiparticle numbers [70].

In the region in-between the flux sweet spots, where the frequency of the qubit is strongly susceptible to flux

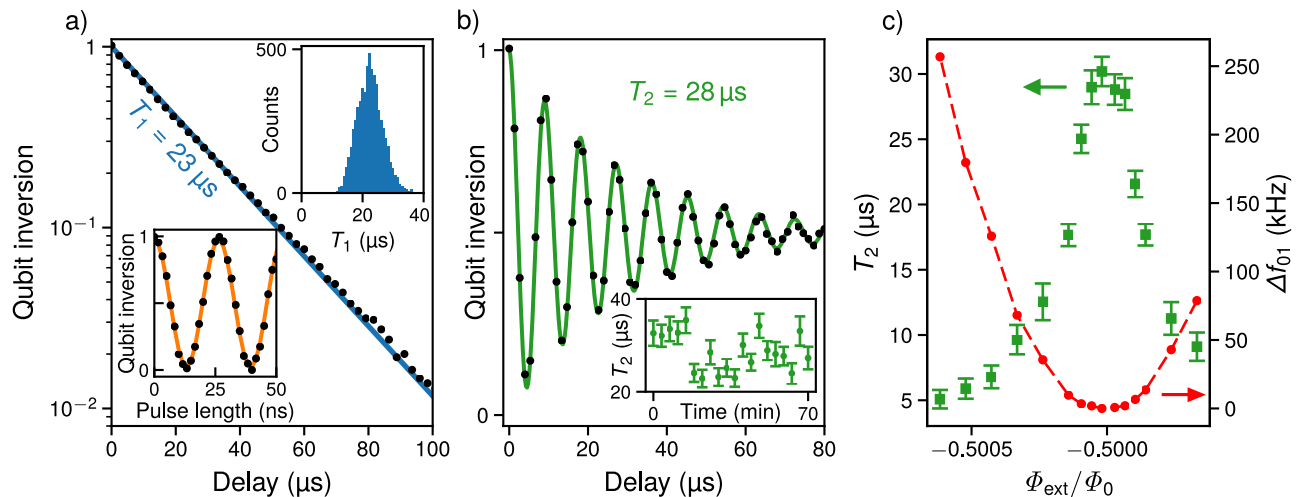


Figure 3. Quantum coherence of the fluxonium superconducting qubit with grAl superinductor. **a)** Average energy relaxation time $T_1 = 23 \mu\text{s}$ at the $\Phi_{\text{ext}}/\Phi_0 = -0.5$ sweet spot, averaged over ~ 6000 measurements taken over a total time of ~ 17 h (measured data - black points, single exponential fit - blue solid line). The histogram in the upper inset shows the distribution of individual T_1 measurements. Rabi oscillations [60] of the qubit with a frequency of 38 MHz, limited by the maximum output power of our microwave generator are shown in the lower inset. A π -pulse, inverting the qubit population, corresponds to a square-envelope pulse with a length of 13 ns. **b)** The black points show the result of a Ramsey fringes measurement [61] for a 110 kHz detuned drive with respect to the qubit frequency of $f_{0.5}^q = 594.37$ MHz at the $\Phi_{\text{ext}}/\Phi_0 = -0.5$ sweet spot, averaged over 70 min. From the fit of an exponentially decaying cosine (green solid line) we extract a coherence time $T_2^{\text{R}} = 28 \mu\text{s}$, comparable to fluxonium qubits with superinductors made from mesoscopic Josephson junction arrays [18, 24, 39, 40]. In the inset, we show the fluctuations of T_2^{R} over time by fitting shorter averaged Ramsey measurements. **c)** Flux dependence of the coherence time T_2^{R} (green squares) and the measured qubit detuning with respect to $f_{0.5}^q$ (red points) close to the half integer sweet spot. The red dashed line connecting the points is a guide to the eye.

noise, T_2 is reduced to values in the range of 50 ns, which could be explained by residual flux noise. The corresponding flux noise amplitude $A = 30 \mu\Phi_0$ is about a factor of three larger than observed in devices using Josephson junction superinductors [71], and it might be due to the longer superinductor loop.

At the zero flux sweet spot, the measured energy decay is non-exponential (see Supplemental Material). It can be fitted to a model assuming a residual decay rate $\Gamma_R = 1/13 \mu\text{s}^{-1}$ and an additional decay $\Gamma_{\text{qp}} = 1/3.2 \mu\text{s}^{-1}$ due to the presence of quasiparticles tunneling across the Josephson junction. From the measured Γ_{qp} we calculate an excess quasiparticle density $x_{\text{qp}} = 1.2 \times 10^{-5}$ in the vicinity of the junction. This excess quasiparticle population can be explained by the larger superconducting gap of grAl (300 μeV) compared to thin film aluminum (230 μeV), which effectively traps quasiparticles. The coherence time $T_2^{\text{R}} = 3.8 \mu\text{s}$ at the zero flux sweet spot is also reduced, as expected from the measured excess quasiparticle population [70].

In summary, we have demonstrated that granular aluminum is a viable material for the implementation of superinductors, and its deposition can be successfully integrated in the fabrication process used for Josephson junctions with pure aluminum electrodes. The measured grAl fluxonium qubit shows state-of-the-art coherence times in the range of tens of μs , while the gate operation time can

be as short as a few ns. If necessary, the currently reported value of the characteristic kinetic inductance of the grAl film, $L_{\text{kin}} = 0.1 \text{ nH}/\square$, can be increased by an order of magnitude by using a thinner and stronger oxidized grAl film. Despite the disordered nature of grAl, a material that incorporates a significant amount of amorphous aluminum oxide, from spectroscopy and time domain measurements we conclude that grAl is a suitable material for superconducting quantum hardware.

We believe that grAl superinductors will enable the realization of increasingly complex, and potentially protected qubit designs. Similarly to the fluxonium qubit, which confines its electromagnetic fields to the parallel plate capacitor of the Josephson junction, and to the internal degrees of freedom of the kinetic inductor, the emerging electronics will be less vulnerable to cross-talk and radiation loss. This could open a new technological avenue towards the up-scaling of quantum coherent superconducting circuits.

We are grateful to A. Bilmes, J. Lisenfeld, C. Smith, W. Wernsdorfer, and M. Wildermuth for insightful discussions, and to J. Ferrero, A. Lukashenko, and L. Radtke for technical assistance. Funding was provided by the Alexander von Humboldt foundation in the framework of a Sofja Kovalevskaja award endowed by the German Federal Ministry of Education and Research, and by the Initiative and Networking Fund of the Helmholtz

Association, within the Helmholtz Future Project *Scalable solid state quantum computing*. This work has been partially supported by the European Research Council advanced grant MoQuOS (N. 741276). I.T. and A.V.U. acknowledge partial support from the Ministry of Education and Science of the Russian Federation in the frame-

work of the Increase Competitiveness Program of the National University of Science and Technology MISIS (Contract No. K2-2017-081). Facilities use was supported by the KIT Nanostructure Service Laboratory (NSL). We acknowledge qKit [72] for providing a convenient measurement software framework.

-
- [1] M. H. Devoret and R. J. Schoelkopf, *Science* **339**, 1169 (2013).
- [2] X. Gu, A. F. Kockum, A. Miranowicz, Y.-x. Liu, and F. Nori, *Phys. Rep.* **718**, 1 (2017).
- [3] R. Barends, A. Shabani, L. Lamata, J. Kelly, A. Mezzacapo, U. L. Heras, R. Babbush, A. G. Fowler, B. Campbell, Y. Chen, Z. Chen, B. Chiaro, A. Dunsworth, E. Jeffrey, E. Lucero, A. Megrant, J. Y. Mutus, M. Neeley, C. Neill, P. J. O'Malley, C. Quintana, P. Roushan, D. Sank, A. Vainsencher, J. Wenner, T. C. White, E. Solano, H. Neven, and J. M. Martinis, *Nature* **534**, 222 (2016).
- [4] P. Roushan, C. Neill, A. Megrant, Y. Chen, R. Babbush, R. Barends, B. Campbell, Z. Chen, B. Chiaro, A. Dunsworth, A. Fowler, E. Jeffrey, J. Kelly, E. Lucero, J. Mutus, P. J. O'Malley, M. Neeley, C. Quintana, D. Sank, A. Vainsencher, J. Wenner, T. White, E. Kapit, H. Neven, and J. Martinis, *Nat. Phys.* **13**, 146 (2016).
- [5] A. Kandala, A. Mezzacapo, K. Temme, M. Takita, M. Brink, J. M. Chow, and J. M. Gambetta, *Nature* **549**, 242 (2017).
- [6] N. K. Langford, R. Sagastizabal, M. Kounalakis, C. Dickel, A. Bruno, F. Luthi, D. J. Thoen, A. Endo, and L. DiCarlo, *Nat. Commun.* **8**, 1715 (2017).
- [7] J. S. Otterbach, R. Manenti, N. Alidoust, A. Bestwick, M. Block, B. Bloom, S. Caldwell, N. Didier, E. S. Fried, S. Hong, P. Karalekas, C. B. Osborn, A. Papageorge, E. C. Peterson, G. Prawiroatmodjo, N. Rubin, C. A. Ryan, D. Scarabelli, M. Scheer, E. A. Sete, P. Sivarajah, R. S. Smith, A. Staley, N. Tezak, W. J. Zeng, A. Hudson, B. R. Johnson, M. Reagor, M. P. da Silva, and C. Rigetti, arXiv:1712.05771 [quant-ph] (2017).
- [8] A. D. King, J. Carrasquilla, J. Raymond, I. Ozfidan, E. Andriyash, A. Berkley, M. Reis, T. Lanting, R. Harris, F. Altomare, K. Boothby, P. I. Bunyk, C. Enderud, A. Fréchet, E. Hoskinson, N. Ladizinsky, T. Oh, G. Poulain-Lamarre, C. Rich, Y. Sato, A. Y. Smirnov, L. J. Swenson, M. H. Volkmann, J. Whittaker, J. Yao, E. Ladizinsky, M. W. Johnson, J. Hilton, and M. H. Amin, *Nature* **560**, 456 (2018).
- [9] N. Ofek, A. Petrenko, R. Heeres, P. Reinhold, Z. Leghtas, B. Vlastakis, Y. Liu, L. Frunzio, S. M. Girvin, L. Jiang, M. Mirrahimi, M. H. Devoret, and R. J. Schoelkopf, *Nature* **536**, 441 (2016).
- [10] D. Ghosh, P. Agarwal, P. Pandey, B. K. Behera, and P. K. Panigrahi, *Quantum Inf. Process.* **17**, 153 (2018).
- [11] N. Roch, M. E. Schwartz, F. Motzoi, C. Macklin, R. Vijay, A. W. Eddins, A. N. Korotkov, K. B. Whaley, M. Sarovar, and I. Siddiqi, *Phys. Rev. Lett.* **112**, 170501 (2014).
- [12] A. Narla, S. Shankar, M. Hatridge, Z. Leghtas, K. M. Sliwa, E. Zalys-Geller, S. O. Mundhada, W. Pfaff, L. Frunzio, R. J. Schoelkopf, and M. H. Devoret, *Phys. Rev. X* **6**, 31036 (2016).
- [13] P. Kurpiers, P. Magnard, T. Walter, B. Royer, M. Pechal, J. Heinsoo, Y. Salathé, A. Akin, S. Storz, J.-C. Besse, S. Gasparinetti, A. Blais, and A. Wallraff, *Nature* **558**, 264 (2018).
- [14] C. Dickel, J. J. Westdorp, N. K. Langford, S. Peiter, R. Sagastizabal, A. Bruno, B. Criger, F. Motzoi, and L. DiCarlo, *Phys. Rev. B* **97**, 64508 (2018).
- [15] J. Koch, T. M. Yu, J. Gambetta, A. A. Houck, D. I. Schuster, J. Majer, A. Blais, M. H. Devoret, S. M. Girvin, and R. J. Schoelkopf, *Phys. Rev. A* **76**, 42319 (2007).
- [16] D. Willsch, M. Nocon, F. Jin, H. De Raedt, and K. Michielsen, *Phys. Rev. A* **96**, 62302 (2017).
- [17] V. E. Manucharyan, J. Koch, L. I. Glazman, and M. H. Devoret, *Science* **326**, 113 (2009).
- [18] I. M. Pop, K. Geerlings, G. Catelani, R. J. Schoelkopf, L. I. Glazman, and M. H. Devoret, *Nature* **508**, 369 (2014).
- [19] S. Gladchenko, D. Olaya, E. Dupont-Ferrier, B. Ducot, L. B. Ioffe, and M. E. Gershenson, *Nat. Phys.* **5**, 48 (2008).
- [20] P. Brooks, A. Kitaev, and J. Preskill, *Phys. Rev. A* **87**, 52306 (2013).
- [21] J. Cohen, W. C. Smith, M. H. Devoret, and M. Mirrahimi, *Phys. Rev. Lett.* **119**, 60503 (2017).
- [22] S. Puri, C. K. Andersen, A. L. Grimsmo, and A. Blais, *Nat. Commun.* **8**, 15785 (2017).
- [23] E. A. Sete, M. J. Reagor, N. Didier, and C. T. Rigetti, *Phys. Rev. Appl.* **8**, 24004 (2017).
- [24] U. Vool, A. Kou, W. C. Smith, N. E. Frattini, K. Serniak, P. Reinhold, I. M. Pop, S. Shankar, L. Frunzio, S. M. Girvin, and M. H. Devoret, *Phys. Rev. Appl.* **9** (2018).
- [25] P. Groszkowski, A. D. Paolo, A. L. Grimsmo, A. Blais, D. I. Schuster, A. A. Houck, and J. Koch, *New J. Phys.* **20**, 043053 (2018).
- [26] I. Chiorescu, Y. Nakamura, C. J. P. M. Harmans, and J. E. Mooij, *Science* **299**, 1869 (2003).
- [27] F. Lecocq, I. M. Pop, I. Matei, E. Dumur, A. K. Feofanov, C. Naud, W. Guichard, and O. Buisson, *Phys. Rev. Lett.* **108**, 107001 (2012).
- [28] F. Yan, S. Gustavsson, A. Kamal, J. Birenbaum, A. P. Sears, D. Hover, T. J. Gudmundsen, D. Rosenberg, G. Samach, S. Weber, J. L. Yoder, T. P. Orlando, J. Clarke, A. J. Kerman, and W. D. Oliver, *Nat. Commun.* **7**, 12964 (2016).
- [29] A. Stockklauser, P. Scarlino, J. V. Koski, S. Gasparinetti, C. K. Andersen, C. Reichl, W. Wegscheider, T. Ihn, K. Ensslin, and A. Wallraff, *Phys. Rev. X* **7**, 11030 (2017).
- [30] N. Samkharadze, G. Zheng, N. Kalhor, D. Brousse, A. Sammak, U. C. Mendes, A. Blais, G. Scappucci, and L. M. K. Vandersypen, *Science* **359**, 1123 (2018).

- [31] A. J. Landig, J. V. Koski, P. Scarlino, U. C. Mendes, A. Blais, C. Reichl, W. Wegscheider, A. Wallraff, K. Ensslin, and T. Ihn, *Nature* **560**, 179 (2018).
- [32] J. J. Viennot, M. C. Dartiailh, A. Cottet, and T. Kontos, *Science* **349**, 408 (2015).
- [33] S. Corlevi, W. Guichard, F. W. J. Hekking, and D. B. Haviland, *Phys. Rev. Lett.* **97**, 96802 (2006).
- [34] T. Weißl, G. Rastelli, I. Matei, I. M. Pop, O. Buisson, F. W. J. Hekking, and W. Guichard, *Phys. Rev. B* **91**, 14507 (2015).
- [35] L. Arndt, A. Roy, and F. Hassler, *Phys. Rev. B* **98**, 14525 (2018).
- [36] J. P. Martinez, S. Leger, N. Gheeraert, R. Dassonneville, L. Planat, F. Foroughi, Y. Krupko, O. Buisson, C. Naud, W. Guichard, S. Florens, I. Snyman, and N. Roch, arXiv:1802.00633 [cond-mat.mes-hall] (2018).
- [37] M. T. Bell, I. A. Sadovskyy, L. B. Ioffe, A. Y. Kitaev, and M. E. Gershenson, *Phys. Rev. Lett.* **109**, 137003 (2012).
- [38] N. A. Masluk, I. M. Pop, A. Kamal, Z. K. Mineev, and M. H. Devoret, *Phys. Rev. Lett.* **109**, 137002 (2012).
- [39] N. Earnest, S. Chakram, Y. Lu, N. Irons, R. K. Naik, N. Leung, L. Ocola, D. A. Czaplewski, B. Baker, J. Lawrence, J. Koch, and D. I. Schuster, *Phys. Rev. Lett.* **120** (2018).
- [40] Y.-H. Lin, L. B. Nguyen, N. Grabon, J. San Miguel, N. Pankratova, and V. E. Manucharyan, *Phys. Rev. Lett.* **120** (2018).
- [41] A. Wallraff, D. I. Schuster, A. Blais, L. Frunzio, R.-S. Huang, J. Majer, S. Kumar, S. M. Girvin, and R. J. Schoelkopf, *Nature* **431**, 162 (2004).
- [42] W. C. Smith, A. Kou, U. Vool, I. M. Pop, L. Frunzio, R. J. Schoelkopf, and M. H. Devoret, *Phys. Rev. B* **94**, 144507 (2016).
- [43] D. Niepce, J. Burnett, and J. Bylander, arXiv:1802.01723 (2018).
- [44] T. M. Hazard, A. Gyenis, A. Di Paolo, A. T. Asfaw, S. A. Lyon, A. Blais, and A. A. Houck, arXiv:1805.00938 (2018).
- [45] J. T. Peltonen, P. C. J. J. Coumou, Z. H. Peng, T. M. Klapwijk, J. S. Tsai, and O. V. Astafiev, *Sci. Rep.* **8** (2018).
- [46] A. Shearrow, G. Koolstra, S. J. Whiteley, N. Earnest, P. S. Barry, F. J. Heremans, D. D. Awschalom, E. Shirokoff, and D. I. Schuster, arXiv:1808.06009 (2018).
- [47] J. Niemeyer, *PTB-Mitteilungen* **84**, 251 (1974).
- [48] G. J. Dolan, *Appl. Phys. Lett.* **31**, 337 (1977).
- [49] G. Deutscher, H. Fenichel, M. Gershenson, E. Grünbaum, and Z. Ovadyahu, *J. Low Temp. Phys.* **10**, 231 (1973).
- [50] U. S. Pracht, N. Bachar, L. Benfatto, G. Deutscher, E. Farber, M. Dressel, and M. Scheffler, *Phys. Rev. B* **93** (2016).
- [51] L. Sun, L. DiCarlo, M. D. Reed, G. Catelani, L. S. Bishop, D. I. Schuster, B. R. Johnson, G. A. Yang, L. Frunzio, L. Glazman, M. H. Devoret, and R. J. Schoelkopf, *Phys. Rev. Lett.* **108**, 230509 (2012).
- [52] H. Rotzinger, S. T. Skacel, M. Pfirrmann, J. N. Voss, J. Münzberg, S. Probst, P. Bushev, M. P. Weides, A. V. Ustinov, and J. E. Mooij, *Supercond. Sci. Technol.* **30**, 25002 (2017).
- [53] L. Grünhaupt, N. Maleeva, S. T. Skacel, M. Calvo, F. Levy-Bertrand, A. V. Ustinov, H. Rotzinger, A. Monfardini, G. Catelani, and I. M. Pop, *Phys. Rev. Lett.* **121**, 117001 (2018).
- [54] N. Maleeva, L. Grünhaupt, T. Klein, F. Levy-Bertrand, O. Dupré, M. Calvo, F. Valenti, P. Winkel, F. Friedrich, W. Wernsdorfer, A. V. Ustinov, H. Rotzinger, A. Monfardini, M. V. Fistul, and I. M. Pop, *Nat. Commun.* **9**, 3889 (2018).
- [55] T. Weißl, B. Küng, E. Dumur, A. K. Feofanov, I. Matei, C. Naud, O. Buisson, F. W. J. Hekking, and W. Guichard, *Phys. Rev. B* **92**, 104508 (2015).
- [56] A. Blais, R.-S. Huang, A. Wallraff, S. M. Girvin, and R. J. Schoelkopf, *Phys. Rev. A* **69** (2004).
- [57] A. Kou, W. C. Smith, U. Vool, I. M. Pop, K. M. Sliwa, M. H. Hatridge, L. Frunzio, and M. H. Devoret, *Phys. Rev. Appl.* **9**, 64022 (2017).
- [58] F. Lecocq, I. M. Pop, Z. Peng, I. Matei, T. Crozes, T. Fournier, C. Naud, W. Guichard, and O. Buisson, *Nanotechnology* **22**, 315302 (2011).
- [59] C. Müller, J. H. Cole, and J. Lisenfeld, arXiv:1705.01108 [cond-mat.mes-hall] (2017).
- [60] I. I. Rabi, *Phys. Rev.* **51**, 652 (1937).
- [61] N. F. Ramsey, *Phys. Rev.* **78**, 695 (1950).
- [62] V. E. Manucharyan, N. A. Masluk, A. Kamal, J. Koch, L. I. Glazman, and M. H. Devoret, *Phys. Rev. B* **85**, 24521 (2012).
- [63] A. Palacios-Laloy, F. Mallet, F. Nguyen, F. Ong, P. Bertet, D. Vion, and D. Esteve, *Phys. Scr.* **T137**, 014015 (2009).
- [64] D. Ristè, C. C. Bultink, M. J. Tiggelman, R. N. Schouten, K. W. Lehnert, and L. DiCarlo, *Nat. Commun.* **4**, 1913 (2013).
- [65] J. Wenner, Y. Yin, E. Lucero, R. Barends, Y. Chen, B. Chiaro, J. Kelly, M. Lenander, M. Mariantoni, A. Megrant, C. Neill, P. J. J. O'Malley, D. Sank, A. Vainsencher, H. Wang, T. C. White, A. N. Cleland, and J. M. Martinis, *Phys. Rev. Lett.* **110**, 150502 (2013).
- [66] S. Gustavsson, F. Yan, G. Catelani, J. Bylander, A. Kamal, J. Birenbaum, D. Hover, D. Rosenberg, G. Samach, A. P. Sears, S. J. Weber, J. L. Yoder, J. Clarke, A. J. Kerman, F. Yoshihara, Y. Nakamura, T. P. Orlando, and W. D. Oliver, *Science* **354**, 1573 (2016).
- [67] K. Serniak, M. Hays, G. de Lange, S. Diamond, S. Shankar, L. D. Burkhardt, L. Frunzio, M. Houzet, and M. H. Devoret, arXiv:1803.00476 [cond-mat.mes-hall] (2018).
- [68] U. Vool, I. M. Pop, K. Sliwa, B. Abdo, C. Wang, T. Brecht, Y. Y. Gao, S. Shankar, M. Hatridge, G. Catelani, M. Mirrahimi, L. Frunzio, R. J. Schoelkopf, L. I. Glazman, and M. H. Devoret, *Phys. Rev. Lett.* **113** (2014).
- [69] P. Kumar, S. Sendelbach, M. A. Beck, J. W. Freeland, Z. Wang, H. Wang, C. C. Yu, R. Q. Wu, D. P. Pappas, and R. McDermott, *Phys. Rev. Applied* **6**, 41001 (2016).
- [70] G. Catelani, S. E. Nigg, S. M. Girvin, R. J. Schoelkopf, and L. I. Glazman, *Phys. Rev. B* **86**, 184514 (2012).
- [71] A. Kou, W. C. Smith, U. Vool, R. T. Brierley, H. Meier, L. Frunzio, S. M. Girvin, L. I. Glazman, and M. H. Devoret, *Phys. Rev. X* **7**, 031037 (2017).
- [72] “qKit - a Quantum Measurement Suite in Python,” <https://github.com/qkitgroup/qkit>.

SUPPLEMENTAL MATERIAL

Coherence times at $\Phi_{\text{ext}} = 0$

The dynamic of the T_1 relaxation shown in Fig. S1a is well described by a sum of two exponential decays. This might be explained by the existence of an additional decay channel, on average present with a probability p_q . The timescale over which this channel influences the energy relaxation needs to be longer than the measurement pulse sequence, which here is $30 \mu\text{s}$. Thus we average measurements with no additional decay resulting in T_r and traces with an additional decay T_q . We fit the measured T_1 relaxation with

$$P(t) = p_q \cdot e^{-\left(\frac{1}{T_q} + \frac{1}{T_r}\right) \cdot t} + (1 - p_q) \cdot e^{-\frac{1}{T_r} \cdot t}. \quad (\text{S1})$$

We attribute this additional decay channel to quasiparticles tunneling across the Josephson junction, similar to [18].

At the $\Phi_{\text{ext}}/\Phi_0 = 0$ sweet spot we measure a coherence time $T_2^{\text{R}} = 3.8 \mu\text{s}$ using a Ramsey fringes measurement [61], about one order of magnitude shorter than at the $\Phi_{\text{ext}}/\Phi_0 = 0.5$ sweet spot (cf. Fig. 3 in the main text). Figure S1c shows T_2^{R} (green squares) and the qubit transition frequency relative to the maximum value of $f_{0,0}^q = 12.540 \text{ GHz}$ (red circles) as a function of the externally applied magnetic flux.

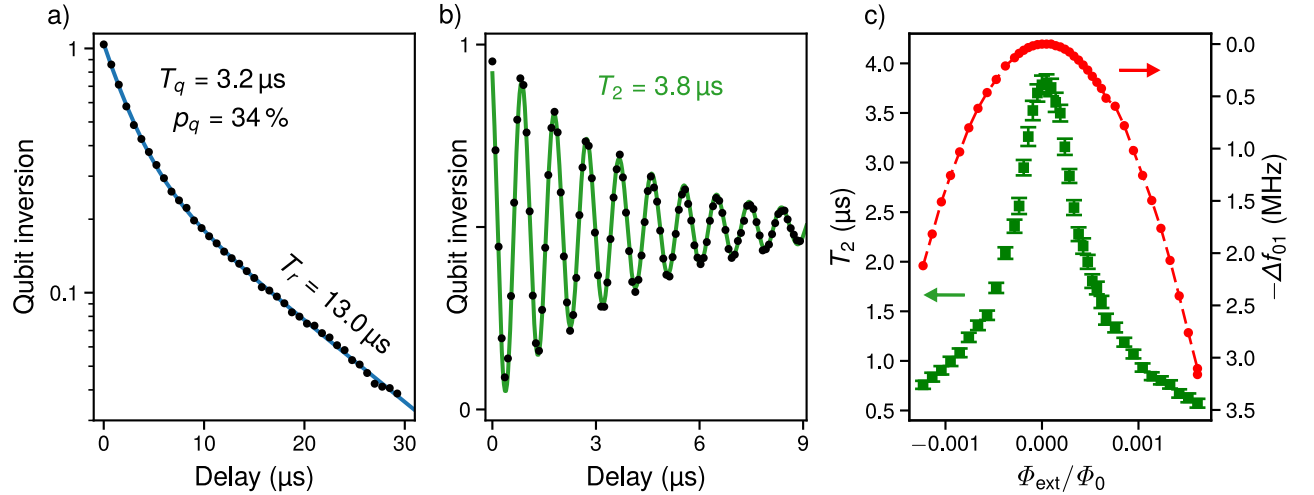


Figure S1. a) Relaxation time T_1 at $\Phi_{\text{ext}} = 0$. The relaxation is well described by a sum of two exponential functions (see Eq. (S1)), assuming time traces with a remaining relaxation time T_r and traces with increased relaxation, at a probability p_q , giving rise to an additional relaxation T_q (measured data - black points, fit - blue solid line) b) The black points show the result of a Ramsey fringes measurement for a 1.15 MHz detuned drive with respect to the qubit frequency of $f_{0,0}^q = 12.540 \text{ GHz}$ at $\Phi_{\text{ext}} = 0$, averaged over 30 min. From the fit of an exponentially decaying cosine (green solid line) we extract a coherence time $T_2^{\text{R}} = 3.8 \mu\text{s}$. c) Flux dependence of the coherence time T_2^{R} (green squares) and the measured qubit detuning (red points) with respect to $f_{0,0}^q$ close to zero flux. The red dashed line connecting the points is a guide to the eye.

Sample fabrication

We fabricated the entire circuit by a three-angle evaporation process using a PMMA/(PMMA-MMA) resist stack on a double-side polished c-plane sapphire substrate. Fig. S2 schematically shows the lithography mask for the Al/AlOx/Al Josephson junction, which is patterned using a 50 keV e -beam writer. The mask combines a Niemeyer-Dolan bridge [47, 48] with an asymmetric undercut [58] for the feedlines. In a first step the Josephson junction is patterned by a two-angle aluminum evaporation process with a thickness of 20 nm and 30 nm, respectively. Thereby, all wires of the design parallel to the evaporation direction, and the antenna, due to its width, are deposited (cf. Fig. 1 in the main text). Finally, without breaking the vacuum, we patterned all inductive parts of the circuit by a zero-angle evaporation of a 40 nm thick grAl film with a resistivity $\rho = 0.8 \times 10^3 \mu\Omega \text{ cm}$. The junction and its feedlines (see Fig. S2 and cf. Fig. 1 in the main text) are connected to the grAl film using connection pads $\sim 2 \mu\text{m}$ away from the Josephson junction.

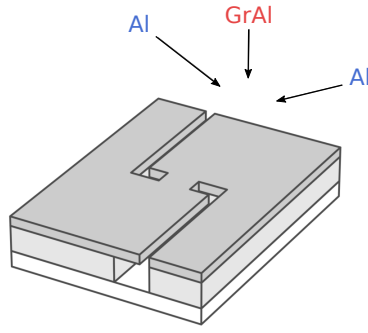


Figure S2. Sketch of the resist stack for structuring the Josephson junction. It combines a Niemeyer-Dolan bridge [47, 48] in its middle with an asymmetric undercut [58] for the feedlines, which are patterned by a double-angle evaporation of pure aluminum. The final zero angle evaporation of grAl does not cover the aluminum film in the vicinity of the Josephson junction and its feedlines. A connection between the junction and the superconductor is ensured by connection pads at the end of the $\sim 2\ \mu\text{m}$ long feedlines (not shown, cf. Fig. 1 in the main text).

Time-domain setup

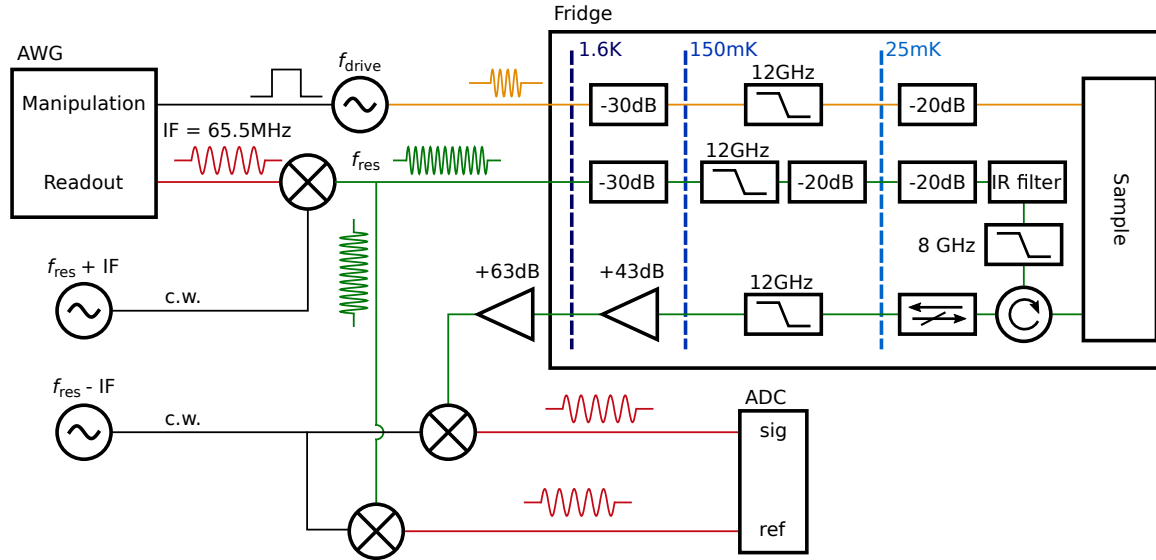


Figure S3. Interferometer setup for time-domain manipulation and measurements. Two separate channels of a commercial arbitrary waveform generator (AWG) provide the pulse shaping abilities for the readout and manipulation pulses. We perform homodyne manipulation by feeding the square envelope pulse from the AWG into the IQ -modulation ports of a commercial microwave vector generator set to the qubit transition frequency. The readout uses a low-cost commercial two-channel microwave generator operated in continuous wave mode in addition to an AWG channel in an interferometric configuration. First, the readout pulse at an intermediate frequency $IF = 65.5\ \text{MHz}$ is upconverted to the readout frequency and split into two signals. One signal is directly measured with the analog digital converter (ADC), whereas the other signal first passes the fridge. Both signals are interfered computationally to extract the I and Q quadratures. All microwave lines in the cryostat are attenuated and filtered using commercially available components. An additional home-made infrared (IR) filter employing Stycast[®], and designed to have an impedance of $50\ \Omega$ at cryogenic temperatures, ensures an attenuation of more than $-10\ \text{dB}$ for frequencies larger than $60\ \text{GHz}$.

Characteristic impedance of the superinductor

From fitting the measured fluxonium spectrum, we obtain a total superinductance of $L_{\text{total}} = 225.6 \text{ nH}$ and a fluxonium capacitance $C_J = 5.2 \text{ fF}$ (see main text), which leads to a qubit plasmon mode impedance of $Z = 6.6 \text{ k}\Omega$. In order to estimate the impedance of the bare superinductor, we measured the Junction size using a SEM image (cf. Fig. 1e in the main text) to be $0.06 \mu\text{m}^2$ with an error of 20%. Using a Josephson junction capacitance per area of $c_J = 50 \text{ fF } \mu\text{m}^{-2}$ we calculate a capacitance of 3 fF for the fluxonium junction alone. This yields a capacitance $C_s = 2.2 \text{ fF}$ associated with the superinductor. Using these values we obtain a superinductor characteristic impedance $Z = \sqrt{L_{\text{total}}/C_s} \approx 10 \text{ k}\Omega$.

For comparison we simulated the superinductor loop, approximating the junction with an ideal capacitor with 3 fF . We obtain a resonant frequency of 5.4 GHz (corresponding to the qubit plasmon mode), from which we calculate a superinductor self capacitance of $C'_s = 0.9 \text{ fF}$. Using this method, the superinductor characteristic impedance is estimated to be $Z = 16 \text{ k}\Omega$. In this simulation, we find the next self-resonant mode of the superinductor at 17.4 GHz , well above the qubit spectrum.